Analysis of RTM extended images for VTI media

Vladimir Li[1], *Ilya Tsvankin*[1] & *Tariq Alkhalifah*[2]
[1]*Center for Wave Phenomena, Colorado School of Mines*
[2]*King Abdullah University of Science and Technology*

SUMMARY

Extended images obtained from reverse-time migration (RTM) contain information about the accuracy of the velocity field and subsurface illumination at different incidence angles. Here, we evaluate the influence of errors in the anisotropy parameters on the shape of the residual moveout (RMO) in P-wave RTM extended images for VTI (transversely isotropic with a vertical symmetry axis) media. Considering the actual spatial distribution of the zero-dip NMO velocity ($V_{\rm nmo}$), which could be approximately estimated by conventional techniques, we analyze the extended images obtained with distorted fields of the parameters η and δ. Differential semblance optimization (DSO) and stack-power estimates are employed to study the sensitivity of focusing to the anisotropy parameters. The results show that the signature of η is dip-dependent, whereas errors in δ cause defocusing only if that parameter is laterally varying. Hence, earlier results regarding the influence of η and δ on reflection moveout and migration velocity analysis remain generally valid in the extended image space for complex media. The dependence of RMO on errors in the anisotropy parameters provides essential insights for anisotropic wavefield tomography using extended images.

INTRODUCTION

The extended imaging condition retains the information about the wavefield directionality and angle-dependent reflector illumination by preserving the spatial and/or temporal correlation lags in the output. For example, one can obtain space-lag (Rickett and Sava, 2002) or time-lag (Sava and Fomel, 2006) extended common-image gathers (CIG), which are the image extensions computed at fixed horizontal coordinates. Sava and Vasconcelos (2009) propose to generate multilag extensions at sparse image points, which significantly reduces the computational cost. These extended common-image-point gathers (CIP) preserve the sensitivity to velocity errors and, therefore, are suitable for velocity model-building.

Wavefield tomography based on minimizing the residual energy at nonzero lags in extended CIGs or CIPs has recently attracted considerable attention in the literature (Yang and Sava, 2011; Li et al., 2014; Weibull and Arntsen, 2014; Yang and Sava, 2015). The defocusing of energy can be quantified using differential semblance optimization (DSO) (Symes and Carazzone, 1991) and/or a measure of stack power (Chavent and Jacewitz, 1995).

Velocity analysis in the extended image domain has significant potential for anisotropic models. The main difficulty in anisotropic imaging is robust estimation of model parameters, and application of wavefield tomography can increase the accuracy of model building in structurally complex areas.

P-wave kinematics in VTI media is controlled by the vertical velocity V_{P0} and Thomsen parameters ε and δ. An alternative parameter set includes the normal-moveout velocity for a horizontal interface ($V_{\rm nmo} = V_{P0}\sqrt{1+2\delta}$), the anellipticity parameter $\eta = (\varepsilon-\delta)/(1+2\delta)$, and δ. Sava and Alkhalifah (2012) analyze extended CIPs obtained with inaccurate values of η in TI media. They consider reflections from a horizontal interface with a constant value of η above it and δ set to zero. They conclude that η-errors cause consistent "V"-shape defocusing regardless of the complexity of the $V_{\rm nmo}$-field.

Here, we evaluate the defocusing in space-lag CIGs and extended CIPs caused by errors in η and δ for VTI models with dipping and curved interfaces and laterally varying δ-fields. The DSO and stack-power objective functions are employed to quantify the defocusing and assess the feasibility of parameter estimation using extended images.

P-WAVE KINEMATICS AND WAVEFIELD RECONSTRUCTION IN VTI MEDIA

Alkhalifah and Tsvankin (1995) demonstrate that P-wave reflection moveout and time-domain processing for a laterally homogeneous VTI medium above the target horizon is controlled by $V_{\rm nmo}$ and η. In the case of a horizontal VTI layer, η controls the nonhyperbolic (long-offset) portion of the P-wave moveout $t(x)$:

$$t^2 = t_0^2 + \frac{x^2}{V_{\rm nmo}^2} - \frac{2\eta x^4}{V_{\rm nmo}^2\,[t_0^2 V_{\rm nmo}^2 + (1+2\eta)x^2]}. \qquad (1)$$

With effective values of $V_{\rm nmo}$ and η, equation 1 remains valid for a stack of horizontal VTI layers above the target horizon (Tsvankin, 2012).

In the reflector beneath a homogeneous VTI layer is dipping, the P-wave NMO velocity depends on both $V_{\rm nmo}$ and η. For typical $\eta > 0$, $V_{\rm nmo}$ increases much faster with dip compared to elliptical ($\varepsilon = \delta$) or purely isotropic models.

P-wave moveout and time-domain processing still depend on just $V_{\rm nmo}$ and η even when these parameters vary laterally above the target horizon, but δ changes only with depth (Alkhalifah et al., 2001). However, if δ is laterally variable, P-wave traveltimes become sensitive to all three relevant parameters - $V_{\rm nmo}$, η, and δ (or V_{P0}, ε, and δ) (Alkhalifah and Tsvankin, 1995; Tsvankin and Grechka, 2011; Tsvankin, 2012).

Inexpensive and kinematically accurate reconstruction of P-wavefields in TI models can be achieved by solving a system of two second-order coupled equations where the velocity V_{S0} is set to zero (Fowler et al., 2010; Duveneck and Bakker, 2011;

DOI http://dx.doi.org/10.1190/segam2015-5930996.1

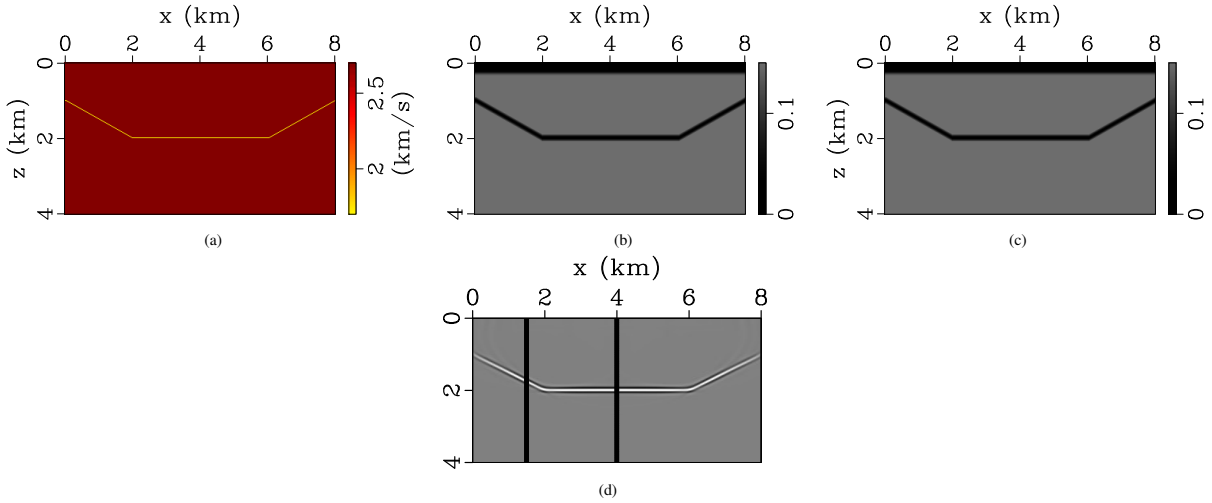

Figure 1: Model with a syncline beneath a homogeneous VTI medium: (a) $V_{\rm nmo}$, (b) η, and (c) δ (model 1). (d) Conventional RTM image obtained with the actual model. The vertical lines mark the locations of extended CIGs (x = 1.5 and 4.0 km).

Zhang et al., 2011). The 2D version of the formulation proposed by Fowler et al. (2010) can be written as:

$$\begin{aligned} \frac{\partial^2 p}{\partial t^2} &= V_{\rm hor}^2 \frac{\partial^2 p}{\partial x^2} + V_{P0}^2 \frac{\partial^2 q}{\partial z^2}, \\ \frac{\partial^2 q}{\partial t^2} &= V_{\rm nmo}^2 \frac{\partial^2 p}{\partial x^2} + V_{P0}^2 \frac{\partial^2 q}{\partial z^2}, \end{aligned} \tag{2}$$

where $V_{\rm hor} = V_{\rm nmo}\sqrt{1+2\eta} = V_{P0}\sqrt{1+2\varepsilon}$ is the P-wave horizontal velocity. Both the p- and q-components contain a wavefield with accurate P-wave kinematics and a shear-wave artifact with a diamond-shape wavefront caused by eliminating V_{S0}. The false shear events in RTM images complicate evaluation of the sensitivity of the focusing to model errors. One way to eliminate the S-wave artifact is to place sources and receivers in a purely isotropic or elliptical ($\varepsilon = \delta$, $\eta = 0$) medium (Alkhalifah, 2000; Duveneck and Bakker, 2011).

SYNTHETIC EXAMPLES

Here, we analyze how the anisotropy parameters η and δ influence the residual moveout in RTM extended images. The parameters $V_{\rm nmo}$, η, and δ are defined on a rectangular grid, and density is assumed to be constant. For all synthetic examples, sources and receivers are located at the surface. The near-surface layer is taken to be isotropic to suppress the shear-wave artifact. We obtain extended CIPs and space-lag CIGs with different η- and δ- fields, while using the actual $V_{\rm nmo}$.

Model 1

In the first test, we evaluate the signature of η for an interface beneath a homogeneous VTI layer. The reflector has a syncline shape with the dip of the flanks equal to 30° (Figure 1).

We scan over η from 0 to 0.3 with a 0.03 increment, while using the actual δ = 0.15. For each value of η, we compute space-lag extended CIGs (Figure 2) and extended CIPs (Figure 3). The residual moveout in both CIGs and CIPs obtained

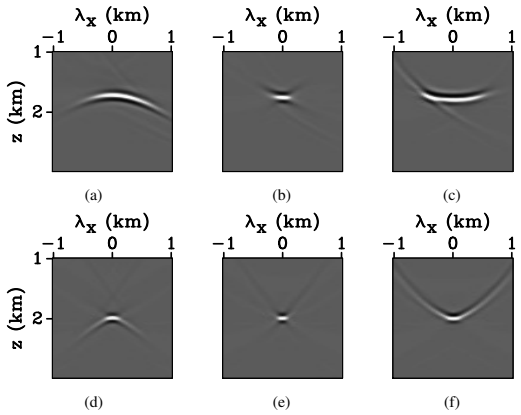

Figure 2: Space-lag CIGs for model 1 computed with η = 0 (a, d), η = 0.15 (b, e), and η = 0.3 (c, f) at: (a-c) x = 1.5 km and (d-f) x = 4.0 km. The actual η = 0.15.

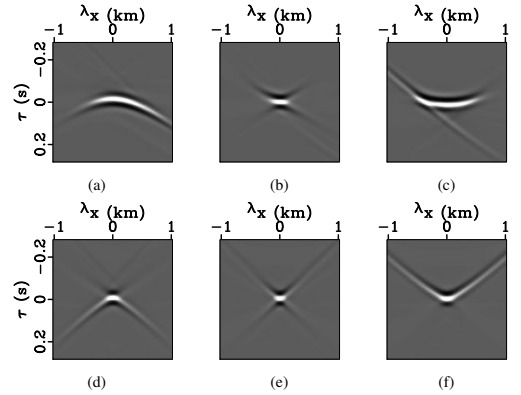

Figure 3: Extended CIPs for model 1 computed with η = 0 (a, d), η = 0.15 (b, e), and η = 0.3 (c, f) at: (a-c) x = 1.5 km and (d-f) x = 4.0 km.

DOI http://dx.doi.org/10.1190/segam2015-5930996.1

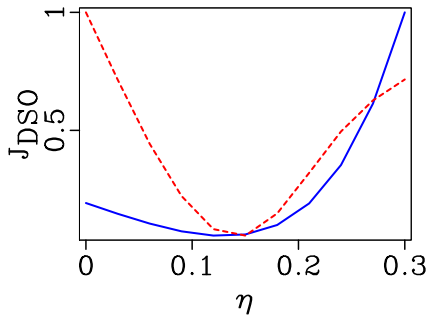

Figure 4: Influence of η on the DSO objective function calculated using space-lag CIGs at: x = 1.5 km (dashed) and x = 4.0 km (solid).

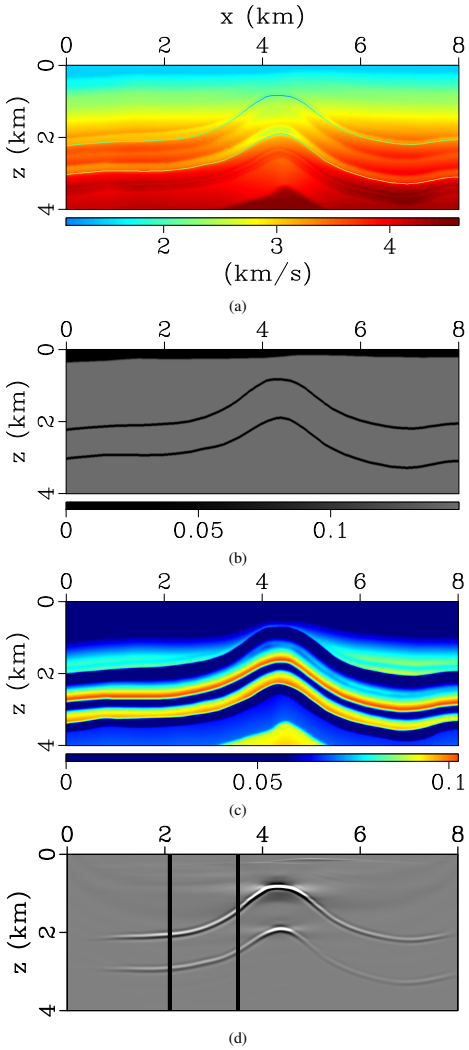

Figure 5: VTI model with an anticline structure (based on a section from the BP 2007 TTI model): (a) V_{nmo}, (b) η, and (c) δ (model 2). (d) Conventional RTM image obtained with the actual parameters. The vertical lines mark locations of extended CIGs (x = 2.1 and 3.5 km).

for the dipping segments of the interface no longer has a "V" shape and resembles the residual caused by an inaccurate velocity model for isotropic media (Figure 2a, c, e; Figure3a, c, e). This is explained by the fact that η changes the NMO velocity and, therefore, conventional-spread moveout for dipping reflectors. To emphasize the dip-dependent influence of η, Figure 4 compares the DSO objective functions for the horizontal (x = 4 km) and dipping (x = 1.5) segments of the interface. Clearly, the energy focusing is more sensitive to the parameter η in the presence of dip.

Model 2

Next, we use a modified segment of the BP 2007 TTI model with an anticline structure (Figure 5). The model, which includes a tilted symmetry axis, was simplified as follows:

- The symmetry-axis tilt is removed to make the model VTI.
- The original V_{nmo}-field is smoothed, and only the two strongest reflectors are retained to avoid reflections from multiple interfaces.
- The parameter η is taken to be constant (η = 0.15) throughout the model.

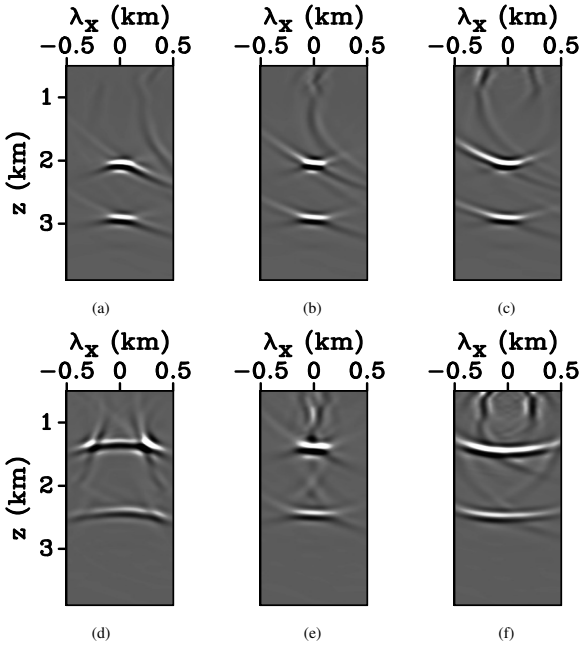

Figure 6: Space-lag CIGs for model 2 computed with η = 0 (a, d), η = 0.15 (b, e), and η = 0.3 (c, f) at: (a, b, c) x = 2.1 km and (d, e, f) x = 3.5 km.

The spatially varying δ-field in the original BP model is left unchanged. We obtain RTM space-lag CIGs for values η ranging from 0 to 0.3 with a 0.05 increment. As in the previous test, the signature of η in space-lag CIGs obtained with the actual δ-field for the dipping interface segments deviates from the "V"-shape (Figure 6d, f). Repeating the test with the erroneous δ = 0 shows that for subhorizontal reflector segments the

DOI http://dx.doi.org/10.1190/segam2015-5930996.1

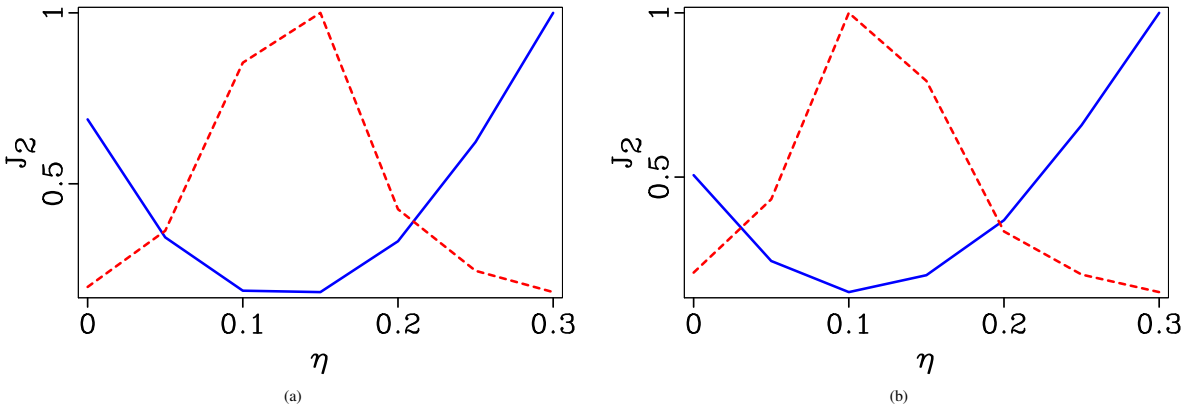

Figure 7: Influence of η on the DSO (solid) and stack-power (dashed) objective functions calculated from space-lag extended images for model 2. The images are obtained with (a) the actual δ-field and (b) $\delta = 0$.

signature of η maintains the "V"-shape even if δ is incorrect. As expected, the RMO in space-lag CIGs for dipping reflector segments due to an error in η does not have the "V"-shape.

The DSO and stack-power objective functions in Figures 7 demonstrate the influence of δ-errors on the sensitivity of the energy focusing to the parameter η. If δ is distorted, the extrema of the DSO and stack-power objective functions are shifted toward lower η-values (close to 0.1).

The gradients of the DSO objective function can be found by applying the adjoint-state method, which involves solving a system of equations adjoint to equations 2. The amplitude and spatial distribution of the adjoint sources are defined by the residual energy in the extended images.

Hence, the deviation of the η-signature from the "V"-shape for dipping interfaces that was identified in the previous example is also observed for this more complicated model. The laterally varying δ influences the focusing in extended images, and, therefore, the shape of the DSO and stack-power objective functions computed as a function of η. However, because for model 2 the lateral variation in δ is relatively mild, that parameter does not change the shape of RMO due to errors in η for both subhorizontal and dipping interface segments.

CONCLUSIONS

We presented a study of the anisotropy signature in RTM extended images for VTI models with dipping interfaces and laterally varying V_{nmo}- and δ-fields. The residual moveout due to errors in η maintains a linear ("V"-like) shape for subhorizontal interfaces, regardless of the complexity of the overburden.

If the reflector is dipping, errors in η lead to more substantial defocusing in the extended image domain, and the shape of the residual moveout is similar to that caused by velocity distortions for isotropic media. The different signature of η for dipping interfaces is explained by the influence of η on NMO velocity, which becomes pronounced for dips reaching 25-30°.

The DSO and stack-power objective functions demonstrate that the energy focusing in extended images is sensitive to the lateral variation of δ. For a simplified segment of the BP TI model, accurate estimation of η from either function requires including δ in the inversion. However, since the lateral variation in δ for the BP model is relatively mild, setting $\delta = 0$ does not noticeably change the shape of RMO caused by η-errors.

The results of our analysis should help design algorithms for VTI tomography in the extended image domain. The ongoing work involves the application of the gradients of the DSO objective function to inversion for the VTI parameters.

ACKNOWLEDGMENTS

We are grateful to Paul Sava (CWP) and members of the A(nisotropy) and I(maging) teams at CWP for fruitful discussions. We also would like to thank Hemang Shah of BP for creating the TTI model (http://www.freeusp.org/2007_BP_Ani_Vel_Benchmark/). This work was supported by the Consortium Project on Seismic Inverse Methods for Complex Structures at CWP. Tariq Alkhalifah thanks KAUST for its support. The reproducible numeric examples in this paper use the Madagascar open-source software package (Fomel et al., 2013) freely available from http://www.ahay.org.

EDITED REFERENCES

Note: This reference list is a copyedited version of the reference list submitted by the author. Reference lists for the 2015 SEG Technical Program Expanded Abstracts have been copyedited so that references provided with the online metadata for each paper will achieve a high degree of linking to cited sources that appear on the Web.

REFERENCES

Alkhalifah, T., 2000, An acoustic wave equation for anisotropic media: Geophysics, **65**, 1239–1250, http://dx.doi.org/10.1190/1.1444815.

Alkhalifah, T., S. Fomel, and B. Biondi, 2001, The space-time domain: Theory and modelling for anisotropic media: Geophysical Journal International, **144**, no. 1, 105–113, http://dx.doi.org/10.1046/j.1365-246x.2001.00300.x.

Alkhalifah, T., and I. Tsvankin, 1995, Velocity analysis for transversely isotropic media: Geophysics, **60**, 1550–1566, http://dx.doi.org/10.1190/1.1443888.

Chavent, G., and C. A. Jacewitz, 1995, Determination of background velocities by multiple migration fitting: Geophysics, **60**, 476–490, http://dx.doi.org/10.1190/1.1443785.

Duveneck, E., and P. M. Bakker, 2011, Stable P-wave modeling for reverse-time migration in tilted TI media: Geophysics, **76**, no. 2, S65–S75, http://dx.doi.org/10.1190/1.3533964.

Fomel, S., P. Sava, I. Vlad, Y. Liu, and V. Bashkardin, 2013, Madagascar: Open-source software project for multidimensional data analysis and reproducible computational experiments: Journal of Open Research Software, **1**, no. 1, http://dx.doi.org/10.5334/jors.ag.

Fowler, P. J., X. Du, and R. P. Fletcher, 2010, Coupled equations for reverse time migration in transversely isotropic media: Geophysics, **75**, no. 1, S11–S22, http://dx.doi.org/10.1190/1.3294572.

Li, Y., B. Biondi, R. Clapp, and D. Nichols, 2014, Wave-equation migration velocity analysis for VTI models: Geophysics, **79**, no. 3, WA59–WA68, http://dx.doi.org/10.1190/geo2013-0338.1.

Rickett, J., and P. Sava, 2002, Offset and angle-domain common image-point gathers for shot-profile migration: Geophysics, **67**, 883–889, http://dx.doi.org/10.1190/1.1484531.

Sava, P., and T. Alkhalifah, 2012, Anisotropy signature in extended images from reverse-time migration: 82nd Annual International Meeting, SEG, Expanded Abstracts, doi:10.1190/segam2012-0124.1.

Sava, P., and S. Fomel, 2006, Time-shift imaging condition in seismic migration: Geophysics, **71**, no. 6, S209–S217, http://dx.doi.org/10.1190/1.2338824.

Sava, P., and I. Vasconcelos, 2009, Efficient computation of extended images by wavefield-based migration: 79th Annual International Meeting, SEG, Expanded Abstracts, 2824–2828.

Symes, W. W., and J. J. Carazzone, 1991, Velocity inversion by differential semblance optimization: Geophysics, **56**, 654–663, http://dx.doi.org/10.1190/1.1443082.

Tsvankin, I., 2012, Seismic signatures and analysis of reflection data in anisotropic media, 3rd ed.: SEG.

Tsvankin, I., and V. Grechka, 2011, Seismology of azimuthally anisotropic media and seismic fracture characterization: SEG, http://dx.doi.org/10.1190/1.9781560802839.

Weibull, W. W., and B. Arntsen, 2014, Anisotropic migration velocity analysis using reverse-time migration: Geophysics, **79**, no. 1, R13–R25, http://dx.doi.org/10.1190/geo2013-0108.1.

Yang, T., and P. Sava, 2011, Wave-equation migration velocity analysis with time-shift imaging: Geophysical Prospecting, **59**, no. 4, 635–650, http://dx.doi.org/10.1111/j.1365-2478.2011.00954.x.

Yang, T., and P. Sava, 2015, Image-domain wavefield tomography with extended common-image-point gathers: Colorado School of Mines Center for Wave Phenomena Report CWP710, http://www.cwp.mines.edu/Documents/cwpreports/CWP710.pdf.

Zhang, Y., H. Zhang, and G. Zhang, 2011, A stable TTI reverse time migration and its implementation: Geophysics, **76**, no. 3, WA3–WA11, http://dx.doi.org/10.1190/1.3554411.